Geometry tagging for heavy ions at JLEIC*

V.S. Morozov[†], **A. Accardi, A. Sy, G.H. Wei**

Thomas Jefferson National Accelerator Facility, Newport News, VA, USA

M.D. Baker

MDBPADS LLC, Miller Place, NY, USA

R. Dupré, M. Ehrhart

IPN Orsay, Orsay, France

C. Fogler, C.E. Hyde

Old Dominion University, Norfolk, VA, USA

P. Nadel-Turonski

Stony Brook University, Stony Brook, NY, USA

J. Stukes

Morehouse College, Atlanta, GA, USA

T. Toll

Shiv Nadar University, Uttar Pradesh, India

L. Zheng

Central China Normal University, Hubei Sheng, China

Geometry tagging is an experimental technique for selecting event samples where one can, on a statistical basis, control the geometry of the collision in order to make more incisive physics measurements. Several physics measurements at the EIC would benefit significantly from the use of this technique, including studies of gluon anti-shadowing, studies of parton propagation, attenuation and hadronization in the nucleus, and ultimately the search for parton saturation. The JLEIC full-acceptance detector, with full acceptance to forward-going neutrons, protons and nuclear fragments and a high data-taking rate is ideally suited to such geometry tagging. We improve, tune, and apply existing modeling codes, BeAGLE, Sartre, and GEMC, and detector descriptions to study this physics.

XXVI International Workshop on Deep-Inelastic Scattering and Related Subjects
16-20 April 2018
Kobe University Convention Centre / Kobe International Conference Center, Kobe, Japan

---

1. Introduction

Electron-nucleus collisions form an essential part of the program for the Electron-Ion Collider (EIC) [1] including studies of gluon anti-shadowing, studies of parton propagation, attenuation and hadronization in the nucleus, and ultimately the search for parton saturation. It greatly benefits from geometry tagging [2], which is an experimental technique for selecting event samples where one can, on a statistical basis, control the geometry of the collision.

The geometry of a nuclear interaction can be defined at high x by the distance "d" traveled by the interacting partons in the nucleus after the first collision and at low x by the impact parameter "b" and the effective nuclear thickness $T(b)$. Figure 1 [3] shows their schematic definitions. Since the back of the nucleus is not a hard edge, the actual definition of d is given by an integral:

$$d = \int_z^\infty \rho(z',b)/\rho_0 dz',$$ (1.1)

where $\rho(z',b)$ is the nuclear density and $\rho_0 = 0.16$ nucleons/fm^3 is the central nuclear density for the *Pb* nucleus, to provide a consistent normalization. The variable d, then, represents the equivalent full density nuclear matter thickness traveled in units of distance (fm). The quantity $\rho_0 d$ is the material thickness traversed in units of nucleons/fm^2.
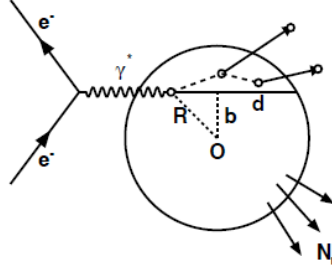

Figure 1: Geometric parameters b, representing the impact parameter, and d, the distance traveled in the nuclear medium after the first collision [3].

The main experimental parameters correlated to the collsion geometry are neutrons produced by evaporation from the excited nuclear remnant after the collision [3, 4, 5], and "knock-out" protons and other charged particles produced during the primary interaction or during the "intranuclear cascade" as remnants of the primary collision re-interact with the rest of the nucleus [6, 7]. The challenge of tagging these forward collision products is that nearby machine elements get in the way of detection. Therefore, the JLEIC full-acceptance detector has been designed in close integration with the machine design of the IR. It relies on a large crossing angle, a set of spectrometer dipoles, large apertures of the final focusing quadrupoles, and a large dispersion combined with a strong focusing of the beam to a small size at the location of a Roman pot detector located after the downstream ion final focusing quads.

2. Geometry tagging for heavy ions at JLEIC

We use BeAGLE [8] (which includes PyQM [9, 10, 11]) as an *eA* event generator to demonstrate the geometry tagging capabilities of the JLEIC full-acceptance detector. Events generated
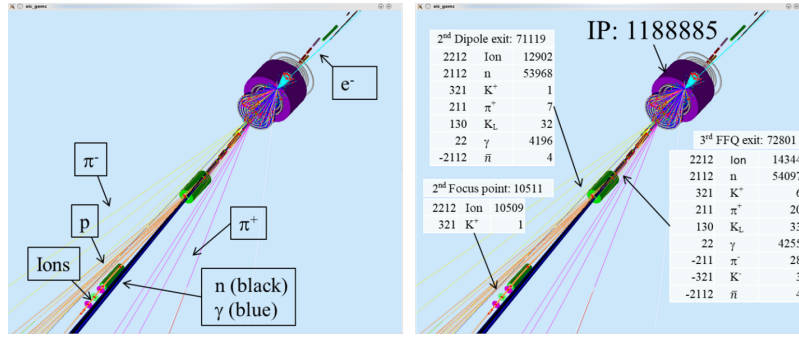
Figure 2: Snapshot of the GEMC event display showing the detector region with tracks from a few BeAGLE events.

by BeAGLE are tracked in a GEMC model of the JLEIC full-acceptance detector to quantify its performance. Figure 2 is a snapshot of the GEMC event display. It shows the detector region with tracks of the final state particles from a few typical BeAGLE events. The different color tracks indicate different particle types and illustrate the detector's acceptance in the far forward direction.

We study, for example, which combination of forward reaction products detectable in JLEIC's full-acceptance detector provides the tightest d cut while maintaining maximumum statistics. Figure 3(left) compares the enhancement of d for different cuts as a function of the cut's statistical efficiency. The selection approaches that we consider and that are listed from top to bottom in the legend of Fig. 3 include: (1) ideal (assuming that d of each event is known), (2) combination of the nuclear remnant's A and Z and the d and α multiplicities, (3) combination of the n, p, d, and α multiplicities, (4) multiplicity of all detectable neutrons, (5) nuclear remnant's A, (6) nuclear remnant's magnetic rigidity, (7) evaporation neutron multiplicity. When cutting based on a combination of the nuclear remnant's A and Z and the d and α multiplicities, we rank each possible combination of these parameters according to its average d and then select the highest-d events on the basis of this rank. The same procedure is applied to other cuts where it is applicable. Figure 3(right) shows the ratios of the first six curves in Fig. 3(left) to the curve for the evaporation neutron multiplicity cut. It illustrates the enhancement of the average d in the first six approaches over that using the
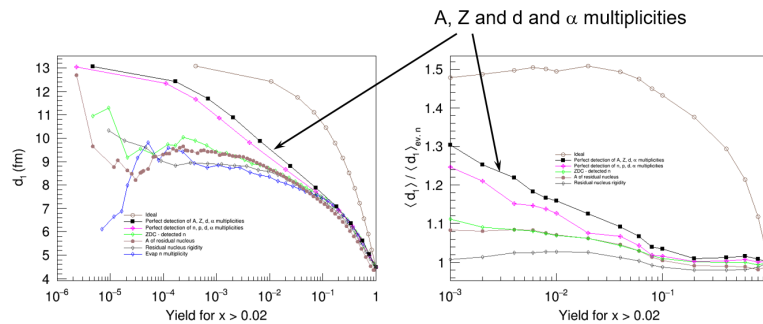

Figure 3: Left: Efficiency of applying various cuts based on detection of the nuclear remnant, multiplicities of different particles and their combinations for enhancing the average d in *ePb* collisions. Right: Enhancement of the average d over that obtained using the evaporation neutron multiplicity cut.

evaporation neutron multiplicity.

Figure 3 shows that geometry tagging based on evaporation neutrons allows one to extend $\langle d_1 \rangle$ from its minimum bias value of about 4.5 to 8 fm with a still reasonable 1% statistics cut. Moreover, a cut on A and Z and the d and α multiplicities further improves this result by about 18%. A and Z of the residual nucleus can be determined by measuring its magnetic rigidity offset (spectrometry) and its charge (energy loss rate). Light ions tend to be sufficiently forward and their detection should not present a problem. A neutron ZDC can provide additional information or a useful measurement on its own. Thus, geometry tagging allows for an incisive study of the propagation of strongly interacting matter in the nucleus by selecting the data with different $\langle d_1 \rangle$ for the same nuclear beam species.

3. Tagging effective nuclear thickness at low x

Geometry tagging at JLEIC is valuable for understanding the transition from a diluted to a saturated gluon state because the higher density for small impact parameter b increases the saturation scale Q_s^2 [12], leading to a corresponding increase in saturation effects. Figure 4(left) adapted from the EIC White Paper [1], is representative of the general structure of $Q_s^2(x,A)$ and can help us qualitatively visualize the value of geometry tagging. The curves represent the saturation scale:

$$Q_s^2 \sim A^{1/3} x^{-\lambda}, \tag{3.1}$$

with $\lambda \simeq 0.3$ for a given value of Bjorken x for four cases: minimum bias ep, minimum bias eCa, minimum bias eAu and central eAu.

The ep and eAu minimum bias curves at fixed x differ by a factor of $A^{1/3}$ (~ 6 for Au), which is often called the nuclear "oomph" factor. At fixed Q^2, the ep and eAu curves differ in x by a factor of about 300. Since the minimum achievable x value at fixed Q^2 is given by $x_{min} \cong Q^2/s_{eN}$, where s_{eN} is the square of the e-nucleon cms collision energy, an eAu collision has a saturation reach similar to an ep collision with a factor 300 larger beam energy ($s \cong 4E_e E_N$). This immediately illustrates the power of using eA collisions to search for saturation effects.

We compare the 1.1% most central bin with the 41.1% most peripheral bin using only the evaporation neutrons (in an ideal detector) from BeAGLE with multinucleon shadowing turned on.
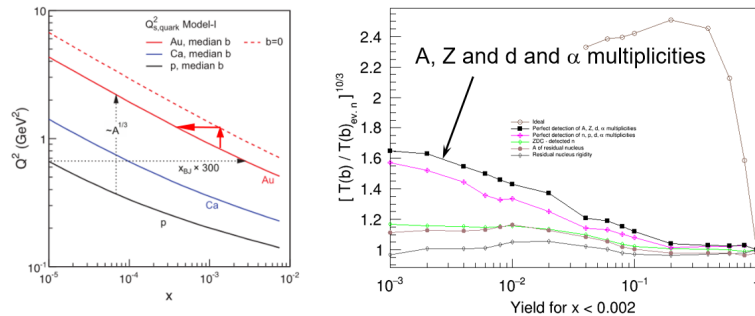

Figure 4: Left: Theoretical expectations for the quark saturation scale for p, minimum bias Ca and Au and central Au. Adapted from Fig 3.9 of Ref. [1]. Right: Enhancement of the effective energy reach over that obtained using the evaporation neutron multiplicity cut.

The average thickness for the central bin is 10.62 fm while for the minimum bias distribution, it is 7.50 fm. This results in a thickness enhancement by a factor of 1.42. This is equivalent to either using an effective A of $\sim$600 or an additional effective shift in E_{beam} of 3.2, for a bin where the geometry tagging is used to enhance the Q_s^2 of the sample. Thus, the impact of the combination of geometry tagging and high luminosity on the reach in Q_s^2 is almost exactly equivalent to an increase of the accelerator energy for *eAu* from 12 on 40 GeV/*A* to 20 on 80 GeV/*A*. It should also be noted that according to the white paper [1], estimates of λ range from $0.2 - 0.3$, which implies that an effective energy enhancement factor could be as high as 5.7. In calculating the factor of 3.2, we used the most conservative value of 0.3.

Using the full-acceptance detector design developed at JLAB, we explore how tagging forward fragments can improve the effective energy reach beyond the dashed line in Fig. 4(left). Figure 4(right) shows that, by using the selection technique described above, one can boost the effective energy reach by another factor of about 1.5 at 1% statistics cut. Moreover, we have shown that using non-spherical nuclei such as ^{238}U can give further energy boost by a factor of about 1.4. These factor are multiplicative and give a total energy boost of $3.2 \times 1.5 \times 1.4 = 6.7$! This demonstrates that advanced detection capabilities and availability of heavy ion beams are essential for the exploration of the parton saturation regime at an EIC.

4. Coherent exclusive diffraction at JLEIC

A powerful probe of gluon saturation is coherent exclusive diffraction: comparing J/ψ and ϕ production in cases where the nucleus remains intact, leading to a quantum mechanical diffraction pattern [13]. The gluon distribution seen by ϕ particles is suppressed at small impact parameters. This can be demonstrated using J/ψ as a control. By measuring this to large values of the target four-momentum transfer, $|t|$, we can obtain a Fourier transform of the gluon distribution in the nucleus. The main challenge of this measurement is that one must be able to tag "truly coherent" events where the nucleus not only remains intact, but also unexcited. This is another measurement where excellent forward detection makes a qualitative difference. Incoherent diffraction, where the nucleus does not remain unaffected, but is excited, is the main background and it needs to be rejected at the level of a factor of $100 - 1000$. Simulations using BeAGLE indicate that more than 10% of incoherent diffractive events yield no evaporation neutrons, so a ZDC-only detection strategy is unlikely to be successful in rejecting this background.

We take a very preliminary first look at vetoing incoherent diffractive events in the JLEIC full-acceptance detector. We use BeAGLE to generate 400k incoherent J/ψ events in 10×40 GeV *ePb* collisions at JLEIC. Our preliminary analysis of these events is presented in Fig. 5. Figure 5(left) shows the incoherent events remaining after the $x < 0.01$ cut, ZDC & Central detector veto, and Full veto. We assume that ZDC vetoes all events containing one or more neutrons and/or high-energy photons ($E_\gamma > 40$ MeV) in the forward acceptance cone of ±10 mrad. The central detector vetoes out all events with one or more neutrons, protons and/or high-energy photons ($E_\gamma > 500$ MeV) with polar angles greater than 100 mrad. The Full veto adds forward protons to the ZDC and Central detector veto. As a zeroth-order approximation, we assume that forward proton acceptance is ±10 mrad.
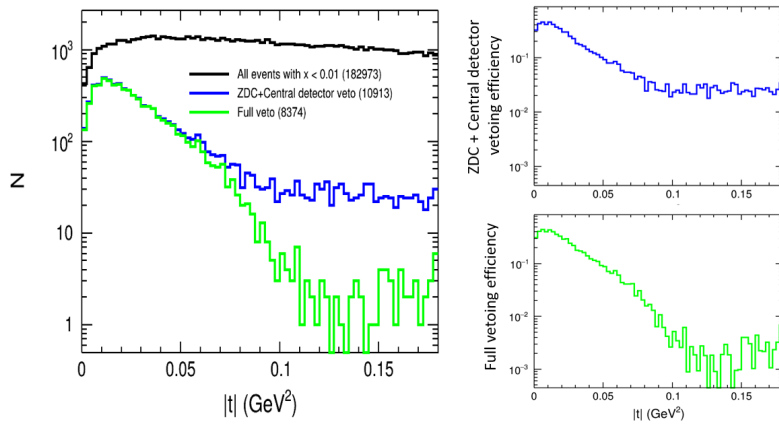
Figure 5: Left: Incoherent J/ψ events in 10×40 GeV *ePb* collisions remaining after the $x < 0.01$ cut, ZDC & Central detector veto, and Full veto. Right: ZDC & Central detector (top) and Full (bottom) vetoing efficiencies.

Comparison of the ZDC & Central detector and Full vetoing efficiencies in Figs. 5(top right) and 5(bottom right), respectively, shows that addition of the forward proton veto takes the vetoing efficiency above $|t|$ of ~ 0.1 GeV^2 from $\sim 10^{-2}$ down to the necessary level of $\sim 10^{-3}$. More realistic simulations of the forward proton acceptance and its vetoing efficiency using an actual detector model are in progress. The acceptance to forward protons is expanded beyond just the apertures of the final focusing quadrupoles using trackers in front of the first final focusing quadrupole. This suggest that the full acceptance design of the JLEIC detector and, in particular, its forward detection capability are indispensable in the search for evidence of parton saturation at low x.

References

[1] A. Accardi *et al.*, *Electron Ion Collider: The Next QCD Frontier*, arXiv:1212.1701v3 [nucl-ex] (2014)

[2] BRAHMS, PHOBOS, STAR, and PHENIX Collaborations, Nucl. Phys. **A757** (2005) 1, 28, 102, 184

[3] L. Zheng, E. C. Aschenauer, and J. H. Lee, Eur. Phys. J. **A50** (2014) 189

[4] M. R. Adams *et al.* (E665 Collaboration), Phys. Rev. Lett. **74** (1995) 5198, & Erratum: Phys. Rev. **80** (1998) 2020

[5] M. Strikman, M. G. Tverskoy, and M. B. Zhalov, Phys. Lett. **B459** (1999) 7

[6] L. Hand *et al.*, Acta Phys. Polon. **B9** (1978) 1087

[7] M. R. Adams *et al.* (E665 Collaboration), Z. Phys. **C65** (1995) 225

[8] https://wiki.bnl.gov/eic/index.php/BeAGLE

[9] R. Dupré, *Quark Fragmentation and Hadron Formation in Nuclear Matter*, Ph.D. thesis (2011), Lyon U.

[10] A. Accardi, Phys. Rev. **C76** (2007) 034902

[11] C. A. Salgado and U. A. Wiedemann, Phys. Rev. **D68** (2003) 014008

[12] H. Kowalski and D. Teaney, Phys. Rev. **D68** (2003) 114005

[13] T. Toll and T. Ullrich, Phys. Rev. **C87** (2013) 024913